NASA/TP-2009-214652

Applications of Ko Displacement Theory to the Deformed Shape Predictions of the Doubly-Tapered Ikhana Wing

William L. Ko, W. Lance Richards, and Van Tran Fleischer
NASA Dryden Flight Research Center
Edwards, California

October 2009

NASA STI Program ... in Profile

Since its founding, NASA has been dedicated to the advancement of aeronautics and space science. The NASA scientific and technical information (STI) program plays a key part in helping NASA maintain this important role.

The NASA STI program operates under the auspices of the Agency Chief Information Officer. It collects, organizes, provides for archiving, and disseminates NASA's STI. The NASA STI program provides access to the NASA Aeronautics and Space Database and its public interface, the NASA Technical Report Server, thus providing one of the largest collections of aeronautical and space science STI in the world. Results are published in both non-NASA channels and by NASA in the NASA STI Report Series, which includes the following report types:

- TECHNICAL PUBLICATION. Reports of completed research or a major significant phase of research that present the results of NASA Programs and include extensive data or theoretical analysis. Includes compilations of significant scientific and technical data and information deemed to be of continuing reference value. NASA counterpart of peer-reviewed formal professional papers but has less stringent limitations on manuscript length and extent of graphic presentations.

- TECHNICAL MEMORANDUM. Scientific and technical findings that are preliminary or of specialized interest, e.g., quick release reports, working papers, and bibliographies that contain minimal annotation. Does not contain extensive analysis.

- CONTRACTOR REPORT. Scientific and technical findings by NASA-sponsored contractors and grantees.

- CONFERENCE PUBLICATION. Collected papers from scientific and technical conferences, symposia, seminars, or other meetings sponsored or co-sponsored by NASA.

- SPECIAL PUBLICATION. Scientific, technical, or historical information from NASA programs, projects, and missions, often concerned with subjects having substantial public interest.

- TECHNICAL TRANSLATION. English-language translations of foreign scientific and technical material pertinent to NASA's mission.

Specialized services also include creating custom thesauri, building customized databases, and organizing and publishing research results.

For more information about the NASA STI program, see the following:

- Access the NASA STI program home page at *http://www.sti.nasa.gov*

- E-mail your question via the Internet to help@sti.nasa.gov

- Fax your question to the NASA STI Help Desk at 443-757-5803

- Phone the NASA STI Help Desk at 443-757-5802

- Write to:
  NASA STI Help Desk
  NASA Center for AeroSpace Information
  7115 Standard Drive
  Hanover, MD 21076-1320

NASA/TP-2009-214652

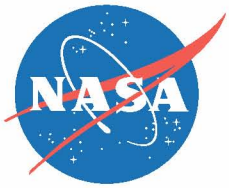

Applications of Ko Displacement Theory to the Deformed Shape Predictions of the Doubly-Tapered Ikhana Wing

William L. Ko, W. Lance Richards, and Van Tran Fleischer
NASA Dryden Flight Research Center
Edwards, California

National Aeronautics and
Space Administration

Dryden Flight Research Center
Edwards, California 93523-0273

October 2009

The structural shape prediction method described in this report is protected under U.S. Patent No. 7,520,176, issued April 21, 2009. Therefore, those interested in using the method should contact the NASA Innovative Partnership Program Office at the Dryden Flight Research Center for more information.

Cover art: NASA Dryden Flight Research Center, photograph number ED07-0186-01.

Available from:

NASA Center for AeroSpace Information
7115 Standard Drive
Hanover, MD 21076-1320
(443) 757-5802

TABLE OF CONTENTS

ABSTRACT

The Ko displacement theory, formulated for weak nonuniform (slowly changing cross sections) cantilever beams, was applied to the deformed shape analysis of the doubly-tapered wings of the Ikhana unmanned aircraft. The two-line strain-sensing system (along the wingspan) was used for sensing the bending strains needed for the wing-deformed shapes (deflections and cross-sectional twist) analysis. The deflection equation for each strain-sensing line was expressed in terms of the bending strains evaluated at multiple numbers of strain-sensing stations equally spaced along the strain-sensing line. For the preflight shape analysis of the Ikhana wing, the strain data needed for input to the displacement equations for the shape analysis were obtained from the nodal-stress output of the finite-element analysis. The wing deflections and cross-sectional twist angles calculated from the displacement equations were then compared with those computed from the finite-element computer program. The Ko displacement theory formulated for weak nonlinear cantilever beams was found to be highly accurate in the deformed shape predictions of the doubly-tapered Ikhana wing.

NOMENCLATURE

c	distance from neutral axis to outermost point of a cross section of uniform beam, in
$c(x)$	distance from neutral axis to outermost point of x-cross section of nonuniform beam, in
c_i	$= c(x_i)$, distance from neutral axis to i-th surfaced strain sensor, in
c_n	value of c_i at wing tip, $x = x_n = l$, in
c_0	value of c_i at wing root, $x = x_0 = 0$, in
d_i	strain-sensing lines separation distance at strain-sensing station, x_i, in
d_n	value of d_i at wing tip, $x = x_n = l$, in
d_0	value of d_i at wing root, $x = x_0 = 0$, in
E	Young's modulus, lb/in^2
h_0	wing root depth at front strain-sensing line, in
h_n	wing tip depth at front strain-sensing line, in
$(h_0)_{\max}$	wing root maximum depth, in
$(h_n)_{\max}$	wing tip maximum depth, in
h_0'	wing root depth at rear strain-sensing line, in
h_n'	wing tip depth at rear strain-sensing line, in
I	moment of inertia, in^4
i	$= 0,1,2,3,...,n$, strain-sensing station identification number
j	dummy index
l	length of wing, in
M	bending moment, in-lb
n	index associated with the last span-wise strain-sensing station
P	applied load, lb
SPAR	Structural Performance And Resizing
T	applied torque, in-lb
w_n	wing tip chord length (width), in
w_0	wing root chord length (width), in
x, y	Cartesian coordinates (x in span-wise direction, y in vertical direction), in
x_i	axial coordinate ($x = x_i$) associated with i-th surface strain sensor (called strain sensing station), in
x_n	strain sensing station at wing tip ($x = x_n = l$), in
x_0	strain sensing station wing root ($x = x_0 = 0$), in
y_i	vertical deflection at $x = x_i$, in

y_0	vertical deflection at wing root ($x = x_0 = 0$), in
Δl	$= l/n$, distance between any two adjacent strain-sensing stations (domain length), in
ε_i	bending strain associated with *i*-th surface strain sensor, in/in
ε_0	bending strain associated with wing root ($i = 0$) surface strain sensor, in/in
θ_i	slope of deformed wing at $x = x_i$, rad or deg
θ_0	slope of deformed wing at wing root ($x = x_0 = 0$), rad or deg
σ_i	stress associated with ε_i, lb/in^2
σ_0	bending stress at wing root upper front strain sensing station, lb/in^2
$\bar{\sigma}_0$	bending stress at wing root lower front strain sensing station, lb/in^2
ϕ_i	cross-sectional twist angle at axial location, $x = x_i$, deg
ϕ_n	cross-sectional twist angle at wing tip ($x = x_n = l$), deg
$( )'$	quantity associated with rear strain-sensing line

INTRODUCTION

In-flight wing-deformed shape monitoring of manned or unmanned aircraft is particularly difficult because of instrumentation weight restrictions. Sensor wiring for conventional strain gage instrumentation is too heavy for many applications where wing shape sensing is desired. Fiber optic sensors offer many advantages over conventional sensor technology because they are lightweight, possess a fine flexible filament form factor (approximately the size of a human hair), and can be highly multiplexed at desired sensing intervals. If multiple strain sensors, such as light-weight fiber optic strain-sensing systems, are installed at discrete sensing stations on a beam-like structure (e.g., aircraft wings), it is possible to use those strain sensor data to input to special displacement equations in order to calculate the deflections and cross-sectional twist angles of a beam-like structure, and thereby predict its deformed shape. The above approach was originally used to develop strain-data-dependent displacement theories for the in-flight deformed shape predictions of the highly flexible, long-span, lightweight, unmanned Helios flying wing (247 ft wingspan; up to 40 ft wing tip deflection).

Based on the classical beam theory, Ko (refs. 1–3) formulated several strain-data-dependent displacement equations for the predictions of deformed shapes (deflections and cross-sectional twist) of cantilever beams (uniform, tapered, slightly-tapered, and step-wisely tapered). The Ko displacement equations were formulated in terms of bending strains evaluated at multiple strain-sensing stations embedded on the surface of the beam. The measured (or finite-element generated) bending strain data are then input to the displacement equations for the calculations of deflections and the cross-sectional twist angle of the beam. When applied to the unmanned aircraft, it is possible for the ground-based pilot to visually monitor the deformed shapes of the aircraft during the flights. The Ko displacement theory together with the onboard fiber optics strain-sensing system could form a powerful tool for in-flight monitoring of the wing shapes by the ground-based pilot for maintaining safe flights of the unmanned aircraft. In addition, the real-time shape monitoring of flexible structures also represents an important step toward the eventual goal of actively controlling the shape of these structures so that they can quickly adapt to their environment while in operation.

This report deals with the preflight deformed shape analysis of the doubly-tapered wings of the Ikhana unmanned research aircraft. Because measured strain data are not yet available, finite-element analysis was used to generate the desired bending strains for inputs to the displacement equations (developed for nonuniform cantilever beams) for the Ikhana wing deformed shape predictions. The Ikhana wing deflections and cross-sectional twist angles calculated from the Ko displacement theory will be compared with those calculated from finite-element analysis, and the accuracy of the displacement theory will be examined.

BASICS OF THE KO DISPLACEMENT THEORY

The formulation of the Ko displacement theory for nonuniform cantilever beams stems from the classical differential equation for the uniform beams given by (refs. 4–5)

$$\frac{d^2y}{dx^2} = \frac{M(x)}{EI} \tag{1}$$

in which y is the vertical displacement, x is the span-wise coordinate, $M(x)$ is the bending moment, E is Young's modulus, and I is the moment of inertia.

Using the bending-stress/moment relationship and Hooke's law, the bending moment $M(x)$ may be written as

$$M(x) = I\frac{\sigma(x)}{c} = EI\frac{\varepsilon(x)}{c} \tag{2}$$

in which c is the uniform beam half depth and $\varepsilon(x)$ is the bending strain at the beam bottom (or top) surface. Substitution of equation (2) into equation (1) yields the following modified beam differential equation

$$\frac{d^2y}{dx^2} = \frac{\varepsilon(x)}{c} \tag{3}$$

Note that, under the present strain formulation, the beam differential equation (3) contains only the beam half depth c and the bending strain $\varepsilon(x)$. The flexural rigidity term EI is eliminated.

The beam differential equation (3) for the uniform beam could be used with sufficient accuracy for nonuniform beams for which the cross-section is assumed to change gradually (ref. 4, p. 143). Replacing the constant half depth c in equation (3) with the varying $c(x)$, one obtains the following modified beam differential equation for nonuniform beams.

$$\frac{d^2y}{dx^2} = \frac{\varepsilon(x)}{c(x)} \tag{4}$$

Equation (4) is the basic equation from which the Ko displacement theory for nonuniform beams was formulated (refs. 1–3). The beam slope and deflection may be obtained by carrying out single and double integrations of equation (4).

Discretization

Using the piece-wise linear assumption and discretizing the beam domain into n sections, and integrating equation (4) (within each beam section) once to obtain the beam slopes, and twice to obtain the beam deflections; Ko (refs. 1–3) formulated the beam slope equations and beam deflection equations for each piece-wise linear section in terms of geometry and bending strains described below.

Let the bottom (or top) surface of the nonuniform beam [length l and varying beam depth $2\,c(x)$] be installed with n +1 bending strain sensors at equally spaced strain-sensing stations x_i (axial coordinate, $x = x_i$), including the fixed end $x_0 (x = 0)$, and the free end $x_n (x = l)$. The nonuniform cantilever beam domain is thus equally divided into n sections with sectional length, $\Delta l = l / n$. The beam is then idealized as a piecewise linearly tapered (either tapering down or tapering up) beam between any two adjacent strain-sensing stations $\{ x_{i-1}, x_i \}$. In the region $x_{i-1} \le x \le x_i$ between the two adjacent strain-sensing stations $\{ x_{i-1}, x_i \}$, the vertical distance $c(x)$ from the neutral surface to the beam bottom (or top) surface, and the bending strain $\{ \varepsilon(x) \}$ may be assumed to be linear functions of x expressed as

$$c(x) = c_{i-1} - (c_{i-1} - c_i) \frac{x - x_{i-1}}{\Delta l} \quad ; \quad x_{i-1} < x < x_i \tag{5}$$

$$\varepsilon(x) = \varepsilon_{i-1} - (\varepsilon_{i-1} - \varepsilon_i) \frac{x - x_{i-1}}{\Delta l} \quad ; \quad x_{i-1} < x < x_i \tag{6}$$

where $\{ c_{i-1}, c_i \}$ and $\{ \varepsilon_{i-1}, \varepsilon_i \}$ are respectively the values of $c(x)$ and $\varepsilon(x)$ at the strain-sensing stations $\{ x_{i-1}, x_i \}$.

Slope Equation

In light of equations (5) and (6), equation (4) may be integrated once (refs. 1, 2, 6) to yield the beam slope $\tan\theta_i$ expressed in equation (7) (see Appendix A for derivation):

$$\tan\theta_i = \frac{\Delta l}{2} \sum_{j=1}^{i} \frac{1}{c_{j-1}} \left[\left(2 - \frac{c_j}{c_{j-1}} \right) \varepsilon_{j-1} + \varepsilon_j \right] + \underbrace{\tan\theta_0}_{=0} \quad ; \quad (i = 1, 2, 3, \ldots, n) \tag{7}$$

Deflection Equation

In light of equations (5) and (6), equation (4) may be integrated twice (refs. 1, 2, 6) to yield the beam deflection y_i expressed in equation (8) (see Appendix A for derivation):

$$y_i = \frac{(\Delta l)^2}{6} \sum_{j=1}^{i} \frac{1}{c_{j-1}} \left\{ \left[3(2j-1) - (3j-2) \frac{c_{i-j+1}}{c_{i-j}} \right] \varepsilon_{i-j} + (3j-2) \varepsilon_{i-j+1} \right\} + \underbrace{y_0 + (i) \Delta l \tan\theta_0}_{=0 \text{ for cantilever beam}} \quad (i = 1, 2, 3, \ldots, n) \tag{8}$$

For the cantilever beam, both the deflection y_0 and the slope $\tan\theta_0$ at the built-in end are zero (i.e., $y_0 = \tan\theta_0 = 0$). The deflection equation (8) will now be used for the Ikhana wing deformed shape analysis with the aid of finite-element analysis.

For the uniform beams $\{ c_i(x) = c \}$, equation (8) degenerates into equation (9) (refs. 1–2)

$$y_i = \frac{(\Delta l)^2}{6c}\left[(3i-1)\varepsilon_0 + 6\sum_{j=1}^{i-1}(i-j)\varepsilon_j + \varepsilon_i \right] + \underbrace{y_0 + (i)\Delta l \tan\theta_0}_{=0 \text{ for cantilever beam}} \qquad (i = 1, 2, 3, \ldots, n) \tag{9}$$

IKHANA UNMANNED AIRCRAFT

Ikhana (fig. 1) is an unmanned science and technology development research aircraft for civilian missions, built by General Atomics Aeronautical Systems Inc., San Diego, California (ref. 7). The aircraft has been named "Ikhana" (ee-kah-nah), a Native American word from the Choctaw Nation meaning intelligent, conscious or aware. The aircraft structure is fabricated with lightweight composite materials, and has a wingspan of 66 ft and a fuselage length of 36 ft. More than 400 lb of sensors can be carried internally and over 2,000 lb in external wing pods. Ikhana is powered by a Honeywell TPE 331-10T turbine engine (Honeywell Aerospace, Phoenix, Arizona) and is capable of reaching altitudes well above 40,000 ft. This aircraft is the first production Predator B equipped with an upgraded digital electronic engine controller (developed by Honeywell and General Atomics Aeronautical Systems Inc.) that will make Ikhana 5-10 percent more fuel-efficient.

The Ikhana aircraft, which is designed for long-endurance and high-altitude flight, will be used for Earth science studies. A variety of atmospheric and remote sensing instruments (e.g., a multi-spectral wildfire sensor), including duplicates of those sensors on orbiting satellites, can be installed to collect data for up to 30 hours.

Ikhana will also be used for advanced aircraft systems research and technology development. Initial experiments will look into the use of fiber optics for wing shape sensing and control, and structural loads measurements.

IKHANA WING GEOMETRY

Figure 1 shows the Ikhana unmanned research aircraft during flight. The Ikhana wing (fig. 2) is a doubly (horizontally and vertically) tapered long cantilever beam. The dimensions of wing length l, wing root and wing tip chord lengths $\{ w_0, w_n \}$, and wing root and wing tip maximum depths $\{ (h_0)_{\max}, (h_n)_{\max} \}$ are listed in table 1.

Table 1. Dimensions of the Ikhana wing.

l, in	w_0, in	w_n, in	$(h_0)_{\max}$, in	$(h_n)_{\max}$, in
360.00	64.80	28.80	12.96	5.76

TWO–LINE STRAIN–SENSING SYSTEM

The two-line strain-sensing system for bending strain sensing (fig. 2), may be used for the deformed shape analysis of the Ikhana wing. Each sensing line contains $n+1$ number of equally spaced strain-sensing stations x_i (i = 0, 1, 2, 3, …, n), including the wing root $x_0 (x = 0)$ and the wing tip $x_n (x = l)$.

Strain–Sensing Line Locations

The installations of front and rear strain-sensing lines are planned on the upper convex surface of the Ikhana wing. Unlike a rectangular cross section with flat lower and upper surfaces, the installations of the two-line strain-sensing system on the upper convex surface of the Ikhana wing require the following technical considerations.

It is desirable to install the strain-sensing lines near the summit of the upper convex surface of the Ikhana wing (small sensing-line-separation distance d_i) in order to obtain larger outputs of bending strains ε_i because the value of c_i, the vertical distance from the neutral surface to the sensing stations, reaches a maximum at the upper surface summit. However, to obtain more accurate data for the cross-sectional twist angle ϕ_i, a larger d_i is desired. But, the larger d_i will decrease the value of c_i because of decreasing wing depth from the summit. The decreased value of c_i will reduce the output of strain ε_i at the same rate under bending moment M according to equation (2). As shown in equation (8), the depth term c_{j-1} is in a denominator, but the strain terms $\{\varepsilon_{i-j}, \varepsilon_{i-j+1}\}$ are in a numerator. Therefore, simultaneous reductions of $[c_{j-1}, \{\varepsilon_{i-j}, \varepsilon_{i-j+1}\}]$ at the same rate of increasing d_i may have little effect on the resulting value of deflection y_i. After exploratory finite-element trade-off studies using different d_i, suitable locations were chosen for the two strain-sensing lines as discussed in the next section.

Figure 2 shows the two strain-sensing lines to be installed at the suitable locations on the upper curved surface of the wing. Each sensing line is to sense the deflections along the sensing line direction. Note that the two strain-sensing lines are not parallel to each other, but separated according to the wing taper rate. The dimensions of sensing-line-separation distances $\{d_0, d_n\}$ at the wing root and wing tip finally determined are given by equation (10),

$$\begin{Bmatrix} d_0 \\ d_n \end{Bmatrix} = \begin{Bmatrix} 18 \\ 8 \end{Bmatrix} \text{ in} \tag{10}$$

which has the taper rate $d_n = 0.4444\, d_0$ identical to the wing taper rate (table 1). The sensing-line-separation distance d_i at any sensing cross section, x_i (i = 0, 1, 2, 3, …, n) is then given by

$$d_i = d_0 - (d_0 - d_n)\frac{x_i}{l} \tag{11}$$

The wing depths under the two sensing lines at the wing root and wing tip are given in table 2. Note that, from table 2, the wing depths under the two strain-sensing lines are slightly less than the associated maximum wing depths, and that the wing depths under the rear strain-sensing line are much closer to the associated maximum wing depths as compared with the wing depths under the front strain-sensing line.

Table 2. Wing depths under two sensing lines.

Wing root		Wing tip	
h_0, in	h_0', in	h_n, in	h_n', in
11.9059 $= 0.9187\,(h_0)_{\max}$	12.5008 $= 0.9646\,(h_0)_{\max}$	5.2915 $= 0.9187\,(h_n)_{\max}$	5.5559 $= 0.9646\,(h_n)_{\max}$

Deflections

The deflections $\{y_i, y_i'\}$ of the front and rear sensing stations lying at the sensing cross section x_i (i = 0,1, 2, 3, …, n) (fig. 2) may be calculated from the deflection equation (8), which is rewritten separately for the front and rear strain-sensing lines as,

Front strain-sensing line:

$$y_i = \frac{(\Delta l)^2}{6}\sum_{j=1}^{i}\frac{1}{c_{i-j}}\left\{\left[3(2j-1)-(3j-2)\frac{c_{i-j+1}}{c_{i-j}}\right]\varepsilon_{i-j}+(3j-2)\varepsilon_{i-j+1}\right\}+\underbrace{y_0+(i)\Delta l\tan\theta_0}_{=0\text{ for cantilever beam}} \qquad (i = 1, 2, 3, \ldots, n) \tag{12}$$

Rear strain-sensing line:

$$y_i' = \frac{(\Delta l)^2}{6}\sum_{j=1}^{i}\frac{1}{c_{i-j}'}\left\{\left[3(2j-1)-(3j-2)\frac{c_{i-j+1}'}{c_{i-j}'}\right]\varepsilon_{i-j}'+(3j-2)\varepsilon_{i-j+1}'\right\}+\underbrace{y_0'+(i)\Delta l\tan\theta_0'}_{=0\text{ for cantilever beam}} \qquad (i = 1, 2, 3, \ldots, n) \tag{13}$$

Equations (12) and (13) respectively give the deflections along the front and rear strain-sensing lines, which for the Ikhana case, are not parallel to each other according to equation (11), and therefore are not in the exact span-wise direction. Because actual measured strain data are not yet available, for the present pre-flight shape analysis, finite-element generated strains will be used as inputs to equations (12) and (13) for the calculations of deflections $\{y_i, y_i'\}$ (see FINITE-ELEMENT ANALYSIS section). It must be mentioned that for upward bending of the Ikhana wing, the induced upper surface bending strains $\{\varepsilon_i, \varepsilon_i'\}$ must be used in equations (12) and (13) to yield positive upward deflections $\{y_i, y_i'\}$.

Cross–Sectional Twist Angle

Using the values of $\{y_i, y_i', d_i\}$, the cross-sectional twist angle ϕ_i at the strain-sensing cross section $x = x_i$ may be calculated from the following cross-sectional twist angle equation,

$$\phi_i = \sin^{-1}\left(\frac{y_i - y_i'}{d_i}\right) \quad ; \quad (i = 0, 1, 2, 3, \ldots, n) \tag{14}$$

which gives zero twist angle $\phi_0 = 0$ (i = 0) at the wing root where $y_0 = 0$ and $y_0' = 0$. The deflections $\{y_i, y_i'\}$ appearing in equation (14) are to be calculated from deflection equations (12) and (13), and d_i is

calculated from equation (11). With the use of equation (14), installations of surface distortion sensors for torsion displacement measurements are not required.

FINITE–ELEMENT ANALYSIS

Before the installations of the two strain-sensing lines to gather the actual strain data for inputs to the displacement equations (12), (13), and (14); either from the ground tests or from the actual Ikhana flight tests, finite-element-generated input strains will be used in the present pre-flight wing shape analysis. The SPAR (Structural Performance And Resizing) finite-element computer program (ref. 8) was used in the finite-element analysis of the Ikhana wing. The SPAR finite-element outputs will provide both nodal stresses and nodal displacements (deflections). Through Hooks's law, the nodal stresses can be converted into nodal strains for input to equations (12), (13), and (14) for the calculations of deflections, which may then be compared with the corresponding deflections (nodal displacements) obtained from the SPAR program.

Ikhana Wing Model

Figure 3 shows the SPAR finite-element model generated for the Ikhana wing, which has 3,639 nodes and 3,632 four-node bending elements. The Ikhana wing model was subjected to combined bending and torsion loading at the wing tip with upward vertical load of $P = 200$ lb and clockwise (increasing angle-of-attack) torque of $T = 1{,}000 \times w_n$ (figs. 2-3).

Finite–Element Strains

If σ_i is the axial stress at the strain-sensing station x_i obtained from the SPAR nodal stress outputs, then the corresponding bending strain ε_i for the input to the deflection equations (12) and (13) may be calculated from Hooke's law

$$\varepsilon_i = \frac{\sigma_i}{E} \tag{15}$$

where E is the Young's modulus.

The deflections calculated from equations (12) and (13) using the SPAR generated finite-element strains (eq. (15)) can then be compared along with the nodal displacements obtained from the SPAR outputs to validate the accuracy of the Ko displacement theory.

Alternatively, using the SPAR displacement outputs, the bending strain ε_i may also be obtained through dividing the element axial nodal displacement differentials by the length of the element at the strain-sensing station x_i (ref. 2). This element-displacement method gave practically identical bending strains as the element-stress method described above (eq. (15)). However, the element-displacement method was found to lose accuracy as the slope of the deflection curve increases toward the wing tip. The SPAR displacement outputs are in reference to the un-deformed wing axis. Therefore, at an increasing slope near the highly bent wing tip, the true tensile strains along the deformed wing axis, when projected on the un-deformed wing axis, may appear as apparent compressive strains near the wing tip. Therefore, the element-displacement method was not used.

CROSS–SECTIONAL NEUTRAL AXIS

To apply the deflection equations (12) and (13), the input strains ε_i and the values of the vertical distances $\{c_i, c_i'\}$ from the front and rear strain-sensing stations $\{x_i, x_i'\}$ to the cross-sectional neutral axis must be known for wing shape predictions. The airfoil geometry (cross-sectional shape) of the Ikhana wing is nonsymmetrical with respect to the neutral axis (fig. 4). If the lower strain sensors were also installed in addition to upper strain sensors, the values of $\{c_i, c_i'\}$ may also be determined experimentally by converting the measured bending strains into surface stresses (positive and negative) through which the zero-stress point may be located (fig. 4). Alternatively, the vertical distances $\{c_i, c_i'\}$ could be determined from the SPAR nodal stress outputs. In the present report, the latter method was used.

Let $\{\sigma_0,\ \bar{\sigma}_0\}$ respectively be the bending stresses (finite-element calculated, or measured) at the upper and lower front strain-sensing stations at the wing root (built-in end), and let h_0 be the vertical distance between the upper and lower wing-root strain-sensing stations, then the values of $c_i = c(x_i)$ at the wing root, $c_0 = c(0)$ may be determined from

$$c_0 = \frac{\sigma_0}{\sigma_0 + \bar{\sigma}_0} h_0 \tag{16}$$

Equation (16) may be written for the rear sensing line using $(\,)'$ symbol as

$$c_0' = \frac{\sigma_0'}{\sigma_0' + \bar{\sigma}_0'} h_0' \tag{17}$$

From the SPAR nodal stress outputs (or actually measured), the values of $\{\sigma_0,\ \bar{\sigma}_0\}$ and $\{\sigma_0',\ \bar{\sigma}_0'\}$ can be found, and the values of $\{c_0, c_0'\}$ may be calculated respectively from equations (16) and (17). The wing tip values $\{c_n, c_n'\}$ may then be obtained by using the wing taper rate as shown in equation (18).

$$\begin{Bmatrix} c_n \\ c_n' \end{Bmatrix} = 0.4444 \begin{Bmatrix} c_0 \\ c_0' \end{Bmatrix} \tag{18}$$

The values of $\{c_0, c_0'\}$ and $\{c_n, c_n'\}$ determined from the SPAR outputs are listed in Table 3.

Table 3. Distance of strain-sensing stations measured from the neutral surface of the wing.

Wing root		Wing tip	
c_0, in	c_0', in	c_n, in	c_n', in
6.4051 $= 0.5380\, h_0$	7.3899 $= 0.5912\, h_0'$	2.8467 $= 0.5380\, h_n$	3.2844 $= 0.5912\, h_n'$

Note that, from table 3, because of the nonsymmetrical wing cross section with respect to the corresponding neutral axis, the magnitudes of $\{c_0, c_0',\ c_n, c_n'\}$ are slightly larger than one half of the respective local wing depth (neutral surface is not the mid-surface).

Finally, the values of $\{c_i, c_i'\}$ at any strain-sensing cross section may then be calculated from the following equations:

$$c_i = c_0 - (c_0 - c_n)\frac{x_i}{l} \tag{19}$$

$$c_i' = c_0' - (c_0' - c_n')\frac{x_i}{l} \tag{20}$$

ACCURACY OF THE KO DISPLACEMENT THEORY

Table 3 lists the bending strains calculated from equation (15) using the SPAR nodal stress outputs (eq. (15)), and the wing deflections calculated from deflection equations (12) and (13), and also from the SPAR program. The bending strains on the upper surface of the wing are compressive strains with negative signs in the SPAR outputs; however, the absolute values of the strain data were used for inputs to the deflection equations (12) and (13) to calculate the upward deflections.

Table 4. Ikhana wing deflections calculated from deflection equations (12), (13), and from the SPAR program; P= 200 lb, T= 1,000 × w_n in-lb.

	Front sensing line			Rear sensing line		
i	ε_i(SPAR), in / in	y_i(Ko), in	y_i(SPAR), in	ε_i'(SPAR), in / in	y_i'(Ko), in	y_i'(SPAR), in
0	0.643810-3	0.000000	0.000000	0.623810-3	0.000000	0.000000
1	0.607619-3	0.102220	0.130155	0.634289-3	0.087930	0.085855
2	0.599048-3	0.412410	0.445820	0.646667-3	0.362560	0.344290
3	0.593333-3	0.942570	0.971055	0.637143-3	0.841590	0.810895
4	0.574762-3	1.708610	1.723180	0.612857-3	1.540140	1.498400
5	0.527619-3	2.723990	2.716775	0.563810-3	2.469490	2.418655
6	0.444762-3	3.991970	3.956860	0.473333-3	3.632580	3.573760
7	0.317143-3	5.497200	5.430535	0.300952-3	4.947445	4.947445
8	0.000000-3	7.178920	7.095200	0.000000-3	6.497190	6.497190

Figure 5 shows the plots of bending strains (absolute values) along the front and rear strain-sensing lines using the SPAR calculated bending strain data listed in table 4. The strain curves are strongly nonlinear and bow shaped because of the effect of double tapering and the cross-sectional shape of the Ikhana wing. Keep in mind that for the case of the classical uniform cantilever beam under tip vertical load, the strain curve is a straight line tapering down toward zero at the beam tip (refs. 4 and 5).

Figure 6 shows the plots of wing deflections using the deflection data presented in table 4. The excellent agreements between the deflection curves calculated from deflection equations (12) and (13), and from the SPAR displacement outputs, implies the high accuracy of the Ko displacement theory.

Table 5 lists the wing cross-sectional twist angles ϕ_i calculated from the cross-sectional angle twist equation (14) and also from the SPAR program.

Table 5. Ikhana wing cross-sectional twist angles ϕ_i calculated from the cross-sectional twist angle equation (14) and from the SPAR program; P= 200 lb, T= 1,000 × w_n in-lb.

i	ϕ_i(Ko),deg	ϕ_i($SPAR$),deg
0	0.00000	0.00000
1	0.04890	0.15154
2	0.18429	0.37531
3	0.40600	0.64399
4	0.74256	0.99077
5	1.24112	1.45392
6	1.96162	2.09106
7	3.00807	2.99392
8	4.57254	4.28736

Figure 7 shows the plots of the cross-sectional twist angle ϕ_i (fig. 3) using the data given in table 5. The correlation between the Ko displacement theory and the SPAR program is again quite good, but is not as close as the deflection curves (fig. 6). The SPAR program gives slightly higher values of ϕ_i than the Ko displacement theory up to the sixth (i = 6) strain-sensing station and then gives slightly lower values beyond the sensing station i = 7. Keep in mind that ϕ_i is extremely sensitive even to the graphically inconspicuous changes in deflections $\{ y_i , y_i' \}$.

CONCLUDING REMARKS

The Ko displacement theory formulated for nonlinear cantilever beams was used to predict the deformed shape of the doubly-tapered unmanned Ikhana aircraft wing. Some important conclusions are given as follows:

1. The two-line strain-sensing system (bending sensor system) is a powerful method for simultaneously sensing the wing bending and torsion displacements without the need of installing surface distortion sensors.

2. The two strain-sensing lines do not have to be parallel to each other, but follow the wing taper rate because each sensing line senses the deflections along the sensing line.

3. To use the Ko displacement theory for shape predictions of a wing with an airfoil cross section, it is necessary to locate the wing cross-sectional neutral axis by means of finite-element analysis (or by direct measurements of top and bottom surface strains), and thereby determine the vertical distance from the sensing stations to the neutral axis (for input to the displacement equations).

4. The wing deflections and twist angles calculated from the Ko displacement theory compared very nicely with the wing deflections and twist angles calculated from the finite-element program.

5. The Ko displacement theory was found to be highly accurate in the deformed shape predictions of the doubly-tapered cantilever beam such as the Ikhana wing.

FIGURES

ED07-0186-01

Figure 1. Ikhana unmanned science and technology development aircraft.

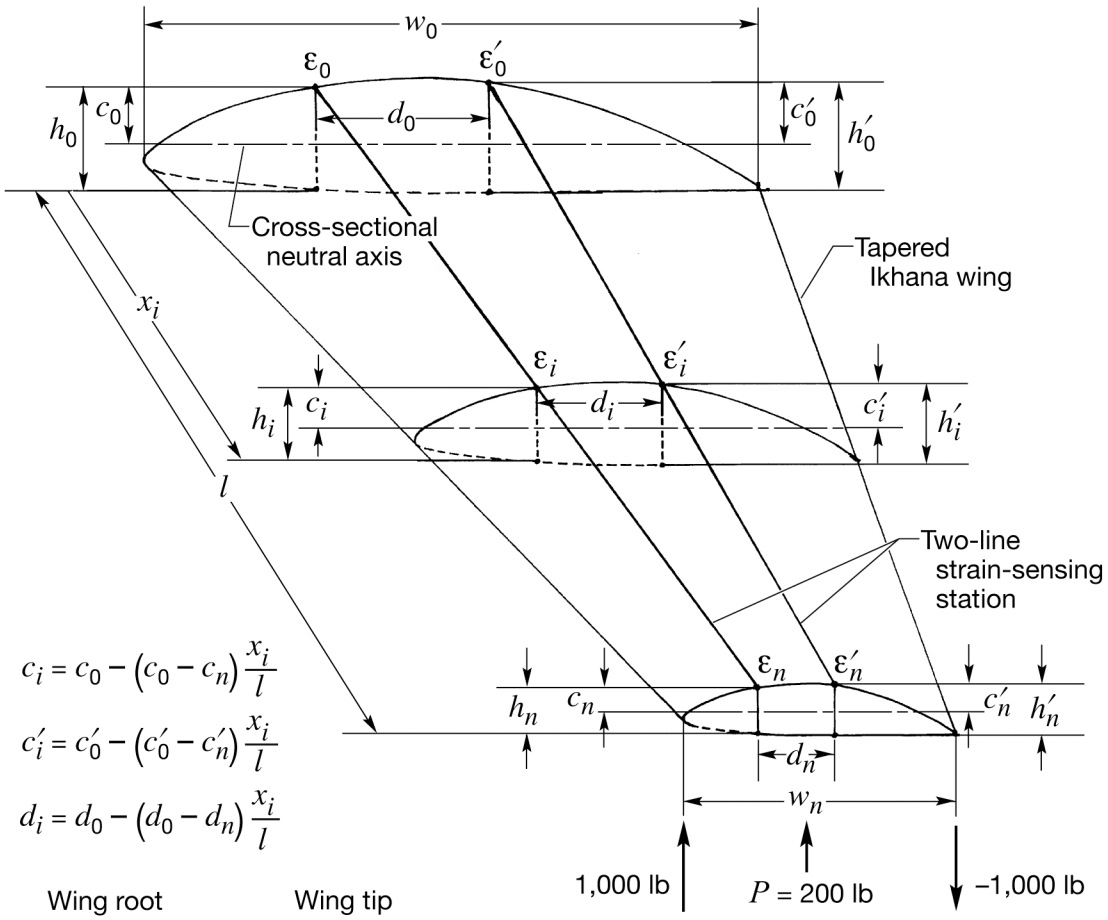

I = 360 in

	Wing root	Wing tip
w	w_0 = 64.8 in	w_n = 28.8 in
d	d_0 = 18.0 in	d_n = 8.0 in
h	h_0 = 11.9059 in	h_n = 5.2915 in
h'	h'_0 = 12.5008 in	h'_n = 5.5559 in
c	c_0 = 6.4051 in	c_n = 2.8467 in
c'	c'_0 = 7.3899 in	c'_n = 3.2844 in

Figure 2. Tapered Ikhana wing installed with a two-line strain-sensing system on the upper surface.

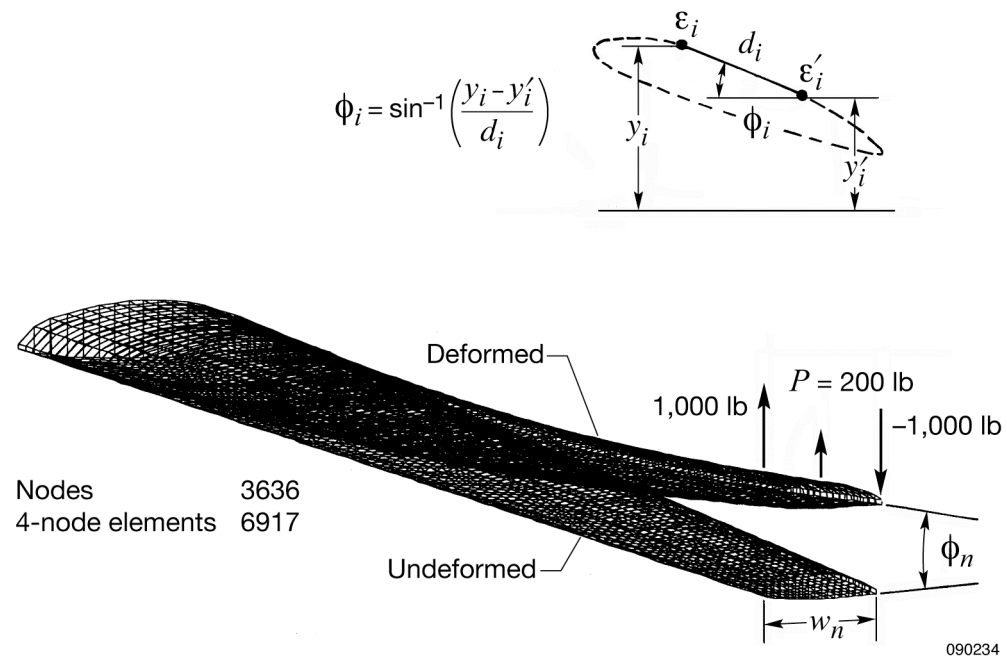

Figure 3. The SPAR finite-element model generated for the Ikhana wing subjected to combined bending and torsion: P = 200 lb; $T = 1{,}000 \times w_n$ in-lb.

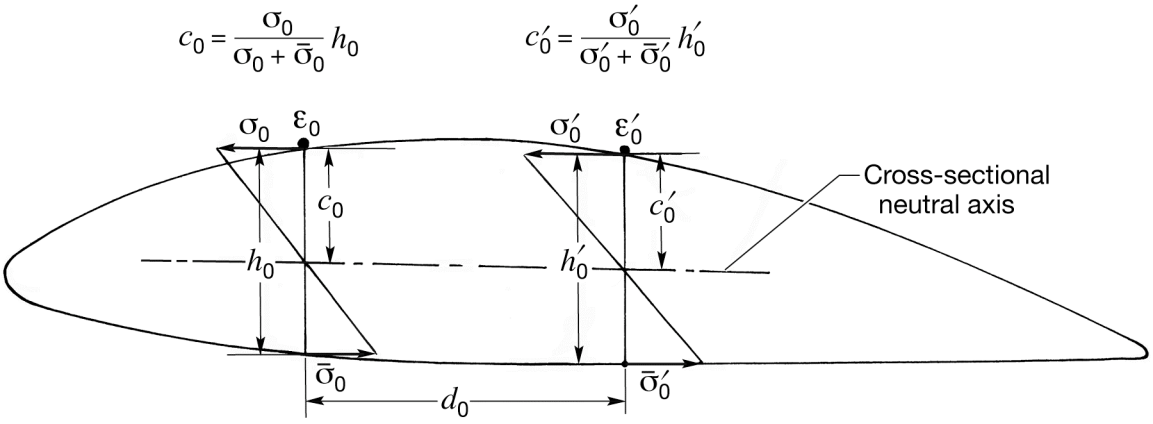

Wing root		Wing tip	
c_0, in	c_0', in	c_n, in	c_n', in
6.4051	7.3899	2.8467	3.2844

Figure 4. Determination of neutral axis for Ikhana wing root cross section using SPAR bending stress outputs.

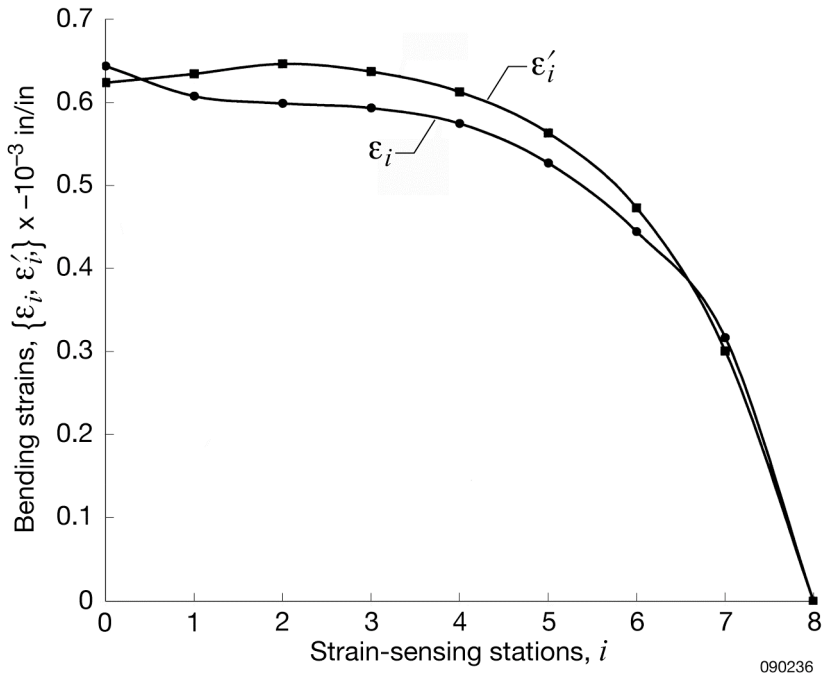

Figure 5. Bending strain curves generated form SPAR element-stress outputs.

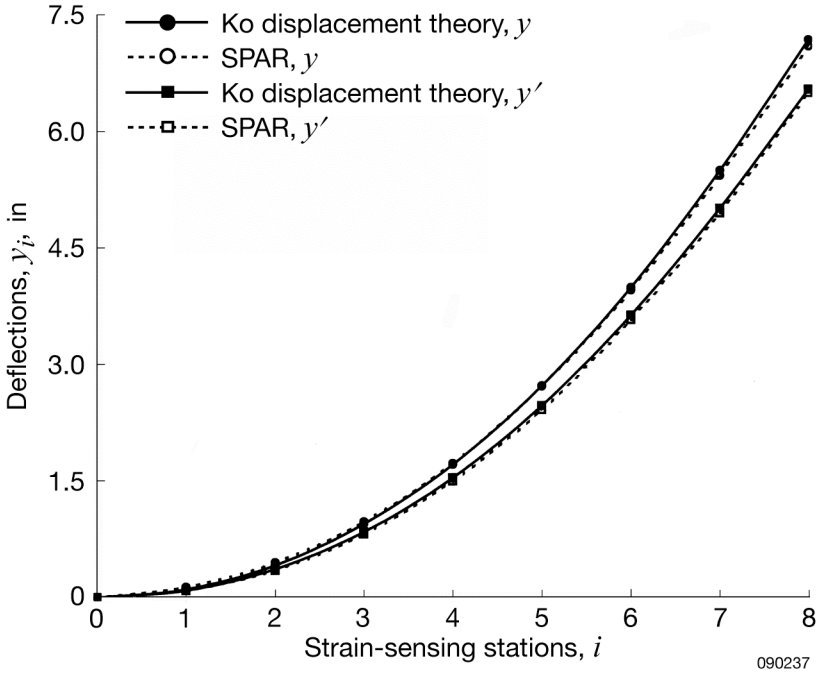

Figure 6. Comparison of Ikhana wing deflections predicted by the Ko displacement theory and calculated by the SPAR analysis.

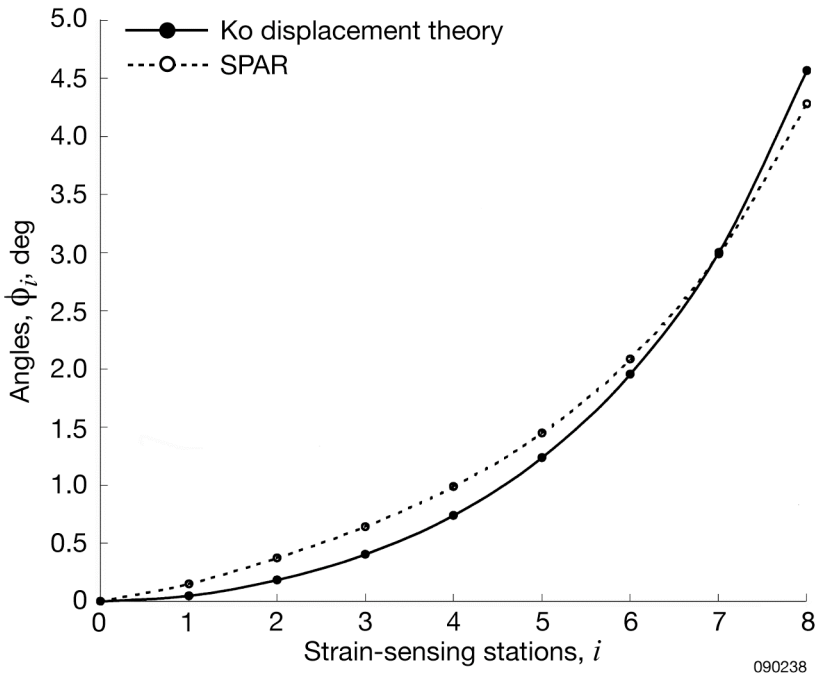

Figure 7. Comparison of the Ikhana wing cross-sectional twist angles predicted by the Ko displacement theory and calculated by the SPAR analysis.

APPENDIX A
DERIVATION OF DEFLECTION EQUATIONS FOR WEAK NONUNIFORM CANTILEVER BEAMS

The deflection equation Ko (ref.1) formulated for weak nonuniform cantilever beams has the following form:

$$y_i = \frac{(\Delta l)^2}{6c_{i-1}}\left[\left(3-\frac{c_i}{c_{i-1}}\right)\varepsilon_{i-1}+\varepsilon_i\right]+y_{i-1}+\Delta l\tan\theta_{i-1} \tag{A1}$$

in which the slope term $\tan\theta_{i-1}$ is expressed as (ref. 1)

$$\tan\theta_{i-1} = \frac{\Delta l}{2c_{i-2}}\left[\left(2-\frac{c_{i-1}}{c_{i-2}}\right)\varepsilon_{i-2}+\varepsilon_{i-1}\right]+\tan\theta_{i-2} \tag{A2}$$

Write out equation (A1) and (A2) for different indices (i = 1-5) as follows:

$$y_1 = \frac{(\Delta l)^2}{6c_0}\left[\left(3-\frac{c_1}{c_0}\right)\varepsilon_0+\varepsilon_1\right]+y_0+\Delta l\tan\theta_0 \quad ; \quad y_0=0\,;\,\Delta l\tan\theta_0=0 \tag{A3a}$$

$$y_2 = \frac{(\Delta l)^2}{6c_1}\left[\left(3-\frac{c_2}{c_1}\right)\varepsilon_1+\varepsilon_2\right]+y_1+\Delta l\tan\theta_1 \quad ; \quad \tan\theta_1=\frac{\Delta l}{2c_0}\left[\left(2-\frac{c_1}{c_0}\right)\varepsilon_0+\varepsilon_1\right]+\tan\theta_0 \tag{A3b}$$

$$y_3 = \frac{(\Delta l)^2}{6c_2}\left[\left(3-\frac{c_3}{c_2}\right)\varepsilon_2+\varepsilon_3\right]+y_2+\Delta l\tan\theta_2 \quad ; \quad \tan\theta_2=\frac{\Delta l}{2c_1}\left[\left(2-\frac{c_2}{c_1}\right)\varepsilon_1+\varepsilon_2\right]+\tan\theta_1 \tag{A3c}$$

$$y_4 = \frac{(\Delta l)^2}{6c_3}\left[\left(3-\frac{c_4}{c_3}\right)\varepsilon_3+\varepsilon_4\right]+y_3+\Delta l\tan\theta_3 \quad ; \quad \tan\theta_3=\frac{\Delta l}{2c_2}\left[\left(2-\frac{c_3}{c_2}\right)\varepsilon_2+\varepsilon_3\right]+\tan\theta_2 \tag{A3d}$$

$$y_5 = \frac{(\Delta l)^2}{6c_4}\left[\left(3-\frac{c_5}{c_4}\right)\varepsilon_4+\varepsilon_5\right]+y_4+\Delta l\tan\theta_4 \quad ; \quad \tan\theta_4=\frac{\Delta l}{2c_3}\left[\left(2-\frac{c_4}{c_3}\right)\varepsilon_3+\varepsilon_4\right]+\tan\theta_3 \tag{A3e}$$

Using the recursion relationships above, one can write out the deflection equation (A1) for different indices as

$$y_2 = \frac{(\Delta l)^2}{6c_1}\left[\left(3-\frac{c_2}{c_1}\right)\varepsilon_1+\varepsilon_2\right]+y_1+\Delta l\tan\theta_1$$

$$= \frac{(\Delta l)^2}{6c_1}\left[\left(3-\frac{c_2}{c_1}\right)\varepsilon_1+\varepsilon_2\right]$$
$$+\overbrace{\frac{(\Delta l)^2}{6c_0}\left[\left(3-\frac{c_1}{c_0}\right)\varepsilon_0+\varepsilon_1\right]+y_0+\Delta l\tan\theta_0}^{y_1}+\overbrace{\frac{(\Delta l)^2}{2c_0}\left[\left(2-\frac{c_1}{c_0}\right)\varepsilon_0+\varepsilon_1\right]+\Delta l\tan\theta_0}^{\tan\theta_1}$$

$$= \frac{(\Delta l)^2}{6c_1}\left[\left(3-\frac{c_2}{c_1}\right)\varepsilon_1+\varepsilon_2\right]+\frac{(\Delta l)^2}{6c_0}\left[\left(9-4\frac{c_1}{c_0}\right)\varepsilon_0+4\varepsilon_1\right]+y_0+2\Delta l\tan\theta_0 \qquad \text{(A4a)}$$

$$y_3 = \frac{(\Delta l)^2}{6c_2}\left[\left(3-\frac{c_3}{c_2}\right)\varepsilon_2+\varepsilon_3\right]+y_2+\Delta l\tan\theta_2$$

$$= \frac{(\Delta l)^2}{6c_2}\left[\left(3-\frac{c_3}{c_2}\right)\varepsilon_2+\varepsilon_3\right]$$
$$+\overbrace{\frac{(\Delta l)^2}{6c_1}\left[\left(3-\frac{c_2}{c_1}\right)\varepsilon_1+\varepsilon_2\right]+\frac{(\Delta l)^2}{6c_0}\left[\left(9-4\frac{c_1}{c_0}\right)\varepsilon_0+4\varepsilon_1\right]+y_0+2\Delta l\tan\theta_0}^{y_2}$$
$$+\overbrace{\frac{(\Delta l)^2}{2c_1}\left[\left(2-\frac{c_2}{c_1}\right)\varepsilon_1+\varepsilon_2\right]+\frac{(\Delta l)^2}{2c_0}\left[\left(2-\frac{c_1}{c_0}\right)\varepsilon_0+\varepsilon_1\right]+\Delta l\tan\theta_0}^{\Delta l\tan\theta_2}$$

$$= \frac{(\Delta l)^2}{6c_2}\left[\left(3-\frac{c_3}{c_2}\right)\varepsilon_2+\varepsilon_3\right]+\frac{(\Delta l)^2}{6c_1}\left[\left(9-4\frac{c_2}{c_1}\right)\varepsilon_1+4\varepsilon_2\right]+\frac{(\Delta l)^2}{6c_0}\left[\left(15-7\frac{c_1}{c_0}\right)\varepsilon_0+7\varepsilon_1\right]$$
$$+y_0+3\Delta l\tan\theta_0 \qquad \text{(A4b)}$$

$$y_4 = \frac{(\Delta l)^2}{6c_3}\left[\left(3-\frac{c_4}{c_3}\right)\varepsilon_3+\varepsilon_4\right]+y_3+\Delta l\tan\theta_3$$

$$= \frac{(\Delta l)^2}{6c_3}\left[\left(3-\frac{c_4}{c_3}\right)\varepsilon_3+\varepsilon_4\right]$$

$$+\overbrace{\frac{(\Delta l)^2}{6c_2}\left[\left(3-\frac{c_3}{c_2}\right)\varepsilon_2+\varepsilon_3\right]+\frac{(\Delta l)^2}{6c_1}\left[\left(9-4\frac{c_2}{c_1}\right)\varepsilon_1+4\varepsilon_2\right]+\frac{(\Delta l)^2}{6c_0}\left[\left(15-7\frac{c_1}{c_0}\right)\varepsilon_0+7\varepsilon_1\right]+y_0+3\Delta l\tan\theta_0}^{y_3}$$

$$+\overbrace{\frac{(\Delta l)^2}{2c_2}\left[\left(2-\frac{c_3}{c_2}\right)\varepsilon_2+\varepsilon_3\right]+\frac{(\Delta l)^2}{2c_1}\left[\left(2-\frac{c_2}{c_1}\right)\varepsilon_1+\varepsilon_2\right]+\frac{(\Delta l)^2}{2c_0}\left[\left(2-\frac{c_1}{c_0}\right)\varepsilon_0+\varepsilon_1\right]+\Delta l\tan\theta_0}^{\Delta l\tan\theta_3}$$

$$= \frac{(\Delta l)^2}{6c_3}\left[\left(3-\frac{c_4}{c_3}\right)\varepsilon_3+\varepsilon_4\right]+\frac{(\Delta l)^2}{6c_2}\left[\left(9-4\frac{c_3}{c_2}\right)\varepsilon_2+4\varepsilon_3\right]+\frac{(\Delta l)^2}{6c_1}\left[\left(15-7\frac{c_2}{c_1}\right)\varepsilon_1+7\varepsilon_2\right]$$

$$+\frac{(\Delta l)^2}{6c_0}\left[\left(21-10\frac{c_1}{c_0}\right)\varepsilon_0+10\varepsilon_1\right]+y_0+4\Delta l\tan\theta_0$$

(A4c)

$$y_5 = \frac{(\Delta l)^2}{6c_4}\left[\left(3-\frac{c_5}{c_4}\right)\varepsilon_4+\varepsilon_5\right]+y_4+\Delta l\tan\theta_4$$

$$= \frac{(\Delta l)^2}{6c_4}\left[\left(3-\frac{c_5}{c_4}\right)\varepsilon_4+\varepsilon_5\right]$$

$$+\overbrace{\left\{\begin{array}{l}\frac{(\Delta l)^2}{6c_3}\left[\left(3-\frac{c_4}{c_3}\right)\varepsilon_3+\varepsilon_4\right]+\frac{(\Delta l)^2}{6c_2}\left[\left(9-4\frac{c_3}{c_2}\right)\varepsilon_2+4\varepsilon_3\right]+\frac{(\Delta l)^2}{6c_1}\left[\left(15-7\frac{c_2}{c_1}\right)\varepsilon_1+7\varepsilon_2\right]\\ \quad+\frac{(\Delta l)^2}{6c_0}\left[\left(21-10\frac{c_1}{c_0}\right)\varepsilon_0+10\varepsilon_1\right]+y_0+4\Delta l\tan\theta_0\end{array}\right.}^{y_4}$$

$$+\overbrace{\left\{\begin{array}{l}\frac{(\Delta l)^2}{2c_3}\left[\left(2-\frac{c_4}{c_3}\right)\varepsilon_3+\varepsilon_4\right]+\frac{(\Delta l)^2}{2c_2}\left[\left(2-\frac{c_3}{c_2}\right)\varepsilon_2+\varepsilon_3\right]+\frac{(\Delta l)^2}{2c_1}\left[\left(2-\frac{c_2}{c_1}\right)\varepsilon_1+\varepsilon_2\right]\\ +\frac{(\Delta l)^2}{2c_0}\left[\left(2-\frac{c_1}{c_0}\right)\varepsilon_0+\varepsilon_1\right]+\Delta l\tan\theta_0\end{array}\right.}^{\Delta l\tan\theta_4}$$

$$= \frac{(\Delta l)^2}{6c_4}\left[\left(3-\frac{c_5}{c_4}\right)\varepsilon_4+\varepsilon_5\right]\frac{(\Delta l)^2}{6c_3}\left[\left(9-4\frac{c_4}{c_3}\right)\varepsilon_3+4\varepsilon_4\right]+\frac{(\Delta l)^2}{6c_2}\left[\left(15-7\frac{c_3}{c_2}\right)\varepsilon_2+7\varepsilon_3\right]$$
$$+\frac{(\Delta l)^2}{6c_1}\left[\left(21-10\frac{c_2}{c_1}\right)\varepsilon_1+10\varepsilon_2\right]+\frac{(\Delta l)^2}{6c_0}\left[\left(27-13\frac{c_1}{c_0}\right)\varepsilon_0+13\varepsilon_1\right]+y_0+5\Delta l\tan\theta_0$$

(A4d)

In summary,

$$y_1 = \frac{(\Delta l)^2}{6c_0}\left[\left(3-\frac{c_1}{c_0}\right)\varepsilon_0+\varepsilon_1\right]+y_0+\Delta l\tan\theta_0 \quad \text{(A5a)}$$

$$y_2 = \frac{(\Delta l)^2}{6c_1}\left[\left(3-\frac{c_2}{c_1}\right)\varepsilon_1+\varepsilon_2\right]+\frac{(\Delta l)^2}{6c_0}\left[\left(9-4\frac{c_1}{c_0}\right)\varepsilon_0+4\varepsilon_1\right]+y_0+2\Delta l\tan\theta_0 \quad \text{(A5b)}$$

$$y_3 = \frac{(\Delta l)^2}{6c_2}\left[\left(3-\frac{c_3}{c_2}\right)\varepsilon_2+\varepsilon_3\right]+\frac{(\Delta l)^2}{6c_1}\left[\left(9-4\frac{c_2}{c_1}\right)\varepsilon_1+4\varepsilon_2\right]+\frac{(\Delta l)^2}{6c_0}\left[\left(15-7\frac{c_1}{c_0}\right)\varepsilon_0+7\varepsilon_1\right]$$
$$+y_0+3\Delta l\tan\theta_0 \quad \text{(A5c)}$$

$$y_4 = \frac{(\Delta l)^2}{6c_3}\left[\left(3-\frac{c_4}{c_3}\right)\varepsilon_3+\varepsilon_4\right]+\frac{(\Delta l)^2}{6c_2}\left[\left(9-4\frac{c_3}{c_2}\right)\varepsilon_2+4\varepsilon_3\right]+\frac{(\Delta l)^2}{6c_1}\left[\left(15-7\frac{c_2}{c_1}\right)\varepsilon_1+7\varepsilon_2\right]$$
$$+\frac{(\Delta l)^2}{6c_0}\left[\left(21-10\frac{c_1}{c_0}\right)\varepsilon_0+10\varepsilon_1\right]+y_0+4\Delta l\tan\theta_0 \qquad \text{(A5d)}$$

$$y_5 = \frac{(\Delta l)^2}{6c_4}\left[\left(3-\frac{c_5}{c_4}\right)\varepsilon_4+\varepsilon_5\right]+\frac{(\Delta l)^2}{6c_3}\left[\left(9-4\frac{c_4}{c_3}\right)\varepsilon_3+4\varepsilon_4\right]+\frac{(\Delta l)^2}{6c_2}\left[\left(15-7\frac{c_3}{c_2}\right)\varepsilon_2+7\varepsilon_3\right]$$
$$+\frac{(\Delta l)^2}{6c_1}\left[\left(21-10\frac{c_2}{c_1}\right)\varepsilon_1+10\varepsilon_2\right]+\frac{(\Delta l)^2}{6c_0}\left[\left(27-13\frac{c_1}{c_0}\right)\varepsilon_0+13\varepsilon_1\right]+y_0+5\Delta l\tan\theta_0 \qquad \text{(A5e)}$$

Based on the indicial progressions in equations (A5a) to (A5e), the following generalized deflection equation for any index i (= 1, 2, 3, …, n) may be established:

$$y_i = \frac{(\Delta l)^2}{6}\sum_{j=1}^{i}\frac{1}{c_{i-j}}\left\{\left[3(2j-1)-(3j-2)\frac{c_{i-j+1}}{c_{i-j}}\right]\varepsilon_{i-j}+(3j-2)\varepsilon_{i-j+1}\right\}+y_0+i\Delta l\tan\theta_0 \qquad \text{(A5f)}$$
$$(i = 1, 2, 3, \ldots, n) \quad ; \quad y_0 = \tan\theta_0 = 0$$

Equation (A5f) is the deflection equation (8) in the text.

Accuracy Checks

The general deflection equation (A5f) will be checked for its accuracy by using i = 4, 5.

For i = 4, equation (A5f) takes on the following form,

$$y_4 = \frac{(\Delta l)^2}{6}\sum_{j=1}^{4}\frac{1}{c_{4-j}}\left\{\left[3(2j-1)-(3j-2)\frac{c_{4-j+1}}{c_{4-j}}\right]\varepsilon_{4-j}+(3j-2)\varepsilon_{4-j+1}\right\}+y_0+4\Delta l\tan\theta_0 \qquad \text{(A6)}$$

which after writing out the summation yields,

$$y_4 = \frac{(\Delta l)^2}{6}\left\{\frac{1}{c_3}\left[\left(3-\frac{c_4}{c_3}\right)\varepsilon_3+\varepsilon_4\right]+\frac{1}{c_2}\left[\left(9-4\frac{c_3}{c_2}\right)\varepsilon_2+4\varepsilon_3\right]+\frac{1}{c_1}\left[\left(15-7\frac{c_2}{c_1}\right)\varepsilon_1+7\varepsilon_2\right]\right.$$
$$\left.+\frac{1}{c_0}\left[\left(21-10\frac{c_1}{c_0}\right)\varepsilon_0+10\varepsilon_1\right]\right\}+y_0+4\Delta l\tan\theta_0 \qquad \text{(A7)}$$

which agrees with equation (A5d) and thus, confirms the accuracy of the general deflection equation (A5f) formulated for slightly nonlinear cantilever beams.

For $i = 5$, equation (A5f) takes on the following form:

$$y_5 = \frac{(\Delta l)^2}{6}\sum_{j=1}^{5}\frac{1}{c_{5-j}}\left\{\left[3(2j-1)-(3j-2)\frac{c_{5-j+1}}{c_{5-j}}\right]\varepsilon_{5-j}+(3j-2)\varepsilon_{5-j+1}\right\}+y_0+5\Delta l\tan\theta_0 \qquad \text{(A8)}$$

Writing out the summations of equation (A8) results in,

$$\begin{aligned} y_5 = {} & \frac{(\Delta l)^2}{6c_4}\left[\left(3-\frac{c_5}{c_4}\right)\varepsilon_4+\varepsilon_5\right]+\frac{(\Delta l)^2}{6c_3}\left[\left(9-4\frac{c_4}{c_3}\right)\varepsilon_3+4\varepsilon_4\right]+\frac{(\Delta l)^2}{6c_2}\left[\left(15-7\frac{c_3}{c_2}\right)\varepsilon_2+7\varepsilon_3\right] \\ & +\frac{(\Delta l)^2}{6c_1}\left[\left(21-10\frac{c_2}{c_1}\right)\varepsilon_1+10\varepsilon_2\right]+\frac{(\Delta l)^2}{6c_0}\left[\left(27-13\frac{c_1}{c_0}\right)\varepsilon_0+13\varepsilon_1\right]+y_0+5\Delta l\tan\theta_0 \end{aligned} \qquad \text{(A9)}$$

which is identical to equation (A5e), and thus validates the accuracy of the general deflection equation (A5f) developed for slightly nonlinear cantilever beams.

REFERENCES

1. Ko, William L., W.L. Richards, and Van T. Tran, *Displacement Theories for In-Flight Deformed Shape Predictions of Aerospace Structures*, NASA/TP-2007-214612, 2007.

2. Ko, William L., *Further Development of Ko Displacement Theory for Deformed Shape Predictions of Nonuniform Aerospace Structures,* NASA/TP-2009-214643, 2009.

3. Ko, William L., and W. Lance Richards, *Method for Real-time Structure Shape-Sensing*, U.S. Patent No. 7,520,176, issued April 21, 2009.

4 Roark, Raymond J., *Formulas for Stress and Strain,* Third Edition, McGraw-Hill Book Company, Inc., New York, 1954.

5. Faupel, Joseph H., *Engineering Design*: *A Synthesis of Stress Analysis and Materials Engineering*, John Wiley and Sons, Inc., New York, 1964.

6. Hodgeman, Charles D., *Standard Mathematical Tables,* Eleventh Edition, Chemical Rubber Publishing Company, Cleveland, Ohio, 1957.

7. Cobleigh, Brent R., *Ikhana: A NASA UAS Supporting Long Duration Earth Science Missions*, NASA/TM-2007-214614, 2007.

8. Whetstone, W.D., *SPAR Structural Analysis System Reference Manual*, System Level 13A, Vol. 1, Program Execution, NASA CR-158970-1, 1978.

REPORT DOCUMENTATION PAGE

Form Approved
OMB No. 0704-0188

1. REPORT DATE *(DD-MM-YYYY)*	2. REPORT TYPE	3. DATES COVERED *(From - To)*
01-10-2009	Technical Publication	

4. TITLE AND SUBTITLE
Applications of Ko Displacement Theory to the Deformed Shape Predictions of the Doubly-Tapered Ikhana Wing

5a. CONTRACT NUMBER

5b. GRANT NUMBER

5c. PROGRAM ELEMENT NUMBER

6. AUTHOR(S)
William L. Ko, W. Lance Richards, and Van Tran Fleischer

5d. PROJECT NUMBER

5e. TASK NUMBER

5f. WORK UNIT NUMBER

7. PERFORMING ORGANIZATION NAME(S) AND ADDRESS(ES)
NASA Dryden Flight Research Center
P.O. Box 273
Edwards, California 93523-0273

8. PERFORMING ORGANIZATION REPORT NUMBER
H-3006

9. SPONSORING/MONITORING AGENCY NAME(S) AND ADDRESS(ES)
National Aeronautics and Space Administration
Washington, DC 20546-0001

10. SPONSORING/MONITOR'S ACRONYM(S)
NASA

11. SPONSORING/MONITORING REPORT NUMBER
NASA/TP-2009-214652

12. DISTRIBUTION/AVAILABILITY STATEMENT
Unclassified -- Unlimited
Subject Category 39 Availability: NASA CASI (443) 757-5802 Distribution: Standard

13. SUPPLEMENTARY NOTES
Ko, Richards, and Fleischer, NASA Dryden Flight Research Center.

14. ABSTRACT

The Ko displacement theory, formulated for weak nonuniform (slowly changing cross sections) cantilever beams, was applied to the deformed shape analysis of the doubly-tapered wings of the Ikhana unmanned aircraft. The two-line strain-sensing system (along the wingspan) was used for sensing the bending strains needed for the wing-deformed shapes (deflections and cross-sectional twist) analysis. The deflection equation for each strain-sensing line was expressed in terms of the bending strains evaluated at multiple numbers of strain-sensing stations equally spaced along the strain-sensing line. For the preflight shape analysis of the Ikhana wing, the strain data needed for input to the displacement equations for the shape analysis were obtained from the nodal-stress output of the finite-element analysis. The wing deflections and cross-sectional twist angles calculated from the displacement equations were then compared with those computed from the finite-element computer program. The Ko displacement theory formulated for weak nonlinear cantilever beams was found to be highly accurate in the deformed shape predictions of the doubly tapered Ikhana wing.

15. SUBJECT TERMS
Ko displacement theory, Deflection equations, Cross-sectional rotation equations, Distributed surface strains, Ikhana wing deformed shape predictions

16. SECURITY CLASSIFICATION OF:			17. LIMITATION OF ABSTRACT	18. NUMBER OF PAGES	19b. NAME OF RESPONSIBLE PERSON
a. REPORT	b. ABSTRACT	c. THIS PAGE			STI Help Desk (email:help@sti.nasa.gov)
					19b. TELEPHONE NUMBER *(Include area code)*
U	U	U	UU	30	(443) 757-5802